Postglacial environmental changes in the northwestern Barents Sea caused by meltwater outbursts

Dhanushka Devendra[1]*, Natalia Szymańska[1], Magdalena Łącka[1], Małgorzata Szymczak-Żyła[1], Magdalena Krajewska[1], Maciej M. Telesiński[1], Marek Zajączkowski[1]

5   [1] Department of Paleoceanography, Institute of Oceanology, Polish Academy of Sciences, Sopot 81-712, Poland

correspondence to: Dhanushka Devendra (devendra@iopan.pl)

Abstract. The last deglaciation was marked by abrupt shifts between cold and warm states reflecting an integrated response to the gradually increasing summer insolation at northern 10 latitudes, changing ocean circulation, and the retreat of the Northern Hemisphere ice sheets. In this study, we present new multiproxy reconstructions of water mass properties and sea surface characteristics from a sediment core from the northwestern Barents Sea (Kveithola) representing the last 14,700 years. Our reconstruction documents four sediment-laden meltwater pulses between 14,700 and 8,200 cal years BP based on biomarkers, stable isotopes, 15 and sedimentological parameters. Deglacial processes primarily cause these meltwater pulses and are possibly supplemented with paleo-lake outbursts, paleo-tsunami currents, or a combination of at least one of these, are characterized by sudden drops in sea surface temperatures, increased sea ice formation, increased terrigenous supply, and a limited influence of Atlantic Water in the northwestern Barents Sea. The influence of the Storegga tsunami, which 20 occurred around the 8,200 cal years BP cooling event likely reached and redistributed the sediment in Kveithola. Strong coarsening of the northwestern Barents shelf was observed after 3,500 years, which might be related to a stronger Atlantic Water inflow from the west across the bank leading to winnowing.

1.   Introduction

30   Meltwater pulses appear to have a distinct and dramatic impact on the climate and oceanography of the European Arctic (Nesje et al., 2004; Harrison et al., 2018; You et al., 2023). Studies reconstructing meltwater pulses and their repercussions gain particular significance in the context of modern climate change, as more meltwater events are anticipated (Harrison et al., 2018; Tuckett et al., 2021). Numerous recent modeling studies have attempted to anticipate the

35   consequences of meltwater discharge from the Antarctic or Greenland ice sheets (Ackermann et al., 2020; Alsos et al., 2022; Nobre et al., 2023; Li et al., 2023). Some predict a slowdown or shutdown of the Meridional Overturning Circulation which would result in severe climatic consequences for the Earth e.g., (Lohmann and Ditlevsen, 2021).

The primary source of deglacial meltwater pulses reaching the Nordic Seas are the

40   Fennoscandian and Svalbard-Barents Sea ice sheets. Uncertainties persist, however, regarding the timelines and intensity of meltwater events occurring through the deglaciation and early Holocene (Harrison et al., 2018; Lucchi et al., 2015; Paus et al., 2019). A study conducted at the depositional mouth fans west of Spitsbergenbanken has shown evidence of two meltwater pulses: MWP-1a0, approximately 19,000 years BP, and MWP-1a, approximately 14,500 years

45   BP (Lucchi et al., 2015). However, there remains a gap in our understanding of meltwater pulses during the Early and mid-Holocene periods.

Situated on the margin of the Barents Sea continental shelf, the Kveithola Trough was shaped by glacial processes (Fig. 1). The Kveithola Trough experiences intense water mass exchange. Its location and latitudinal orientation cause it to host AW flowing into the Barents Sea (Rumohr

50   et al., 2001). The trough also acts as a conduit for cold, saline bottom waters laden with sediment, which descend from Spitsbergenbanken to the continental slope (Fohrmann et al., 1998) (Fig. 1c). How these water masses interact varies based on the strength of AW advection, sea-ice distribution, and local oceanographic conditions.

Previous studies at the Kveithola Trough have focused on seismic stratigraphy e.g., (Rüther et

55   al., 2012; Rebesco et al., 2016; Bjarnadóttir et al., 2012). Paleoceanographic investigations exists from the eastern, upper section of the trough, covering the last ~12,000 years e.g., (Belt et al., 2015; Berben et al., 2014; Groot et al., 2014). Here we present a sedimentary record spanning the past 14,700 years from the lower, western, portion of the Kveithola Trough. The location, situated in the west of the depositional fan allowed for the acquisition of a record

60   preserved in a steady environment (Fig. 1). At the same time the western part of the trough is deep enough (>350m) to be unaffected by seabed erosion by icebergs (Lucchi et al., 2015). We

Climate
of the Past
Discussions

have implemented an array of proxies ranging from biomarkers to micropaleontological assemblages to best reconstruct the paleoenvironment and discern the presence and impact of meltwater pulses at Northwestern (NW) Barents Sea.
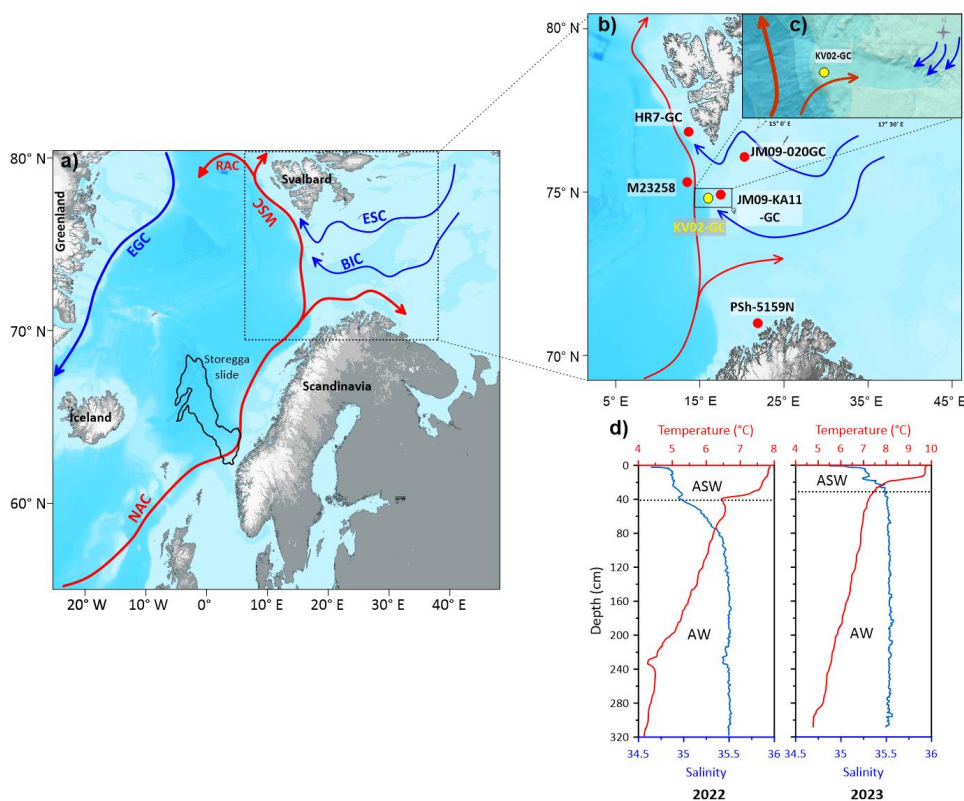
65

Figure 1: (a) Present-day surface ocean circulation in the Nordic Seas. The black polygon shows the extent of the Storegga slide (Bondevik et al., 2005). (b) Locations of marine sediment cores mentioned in the text: OCE2022-KV2-GC (this study), HR7-GC (Devendra et al., 2023), JM09-020-GC (Łącka et al., 2019), M23258 (Sarnthein et al., 2003), JM09-KA11-GC (Berben et al., 2014) and PSh-5159N (Risebrobakken et

70 **al., 2010). (c) Bathymetry map of the Kveithola Trough. The red arrows represent the flow of warm Atlantic Water, i.e., North Atlantic Current (NAC), West Spitsbergen Current (WSC), and Return Atlantic Current (RAC). The blue arrows represent the East Greenland Current (EGC), East Spitsbergen Current (ESC), and the Bear Island Current (BIC). (d) Salinity, temperature, and depth profiles were measured in August 2022 and August 2023 at the core site of OCE2022-KV02-GC (temperature in red and salinity in blue).**

75 **Abbreviations: ASW – Arctic Surface Water; AW – Atlantic Water.**

2.   Regional setting

The western Barents Sea and west Spitsbergen continental margins direct the northward propagating Norwegian Atlantic Current (NwAC). The NwAC moves from the south, carrying

warm and salty Atlantic Water (T > 3 °C, S > 35.0) into the Nordic Seas (Smedsrud et al., 2021; Hopkins, 1991). It then spreads into the Barents Sea through North Cape Current (NCaC), and into the Arctic Ocean via the West Spitsbergen Current (Fig. 1). Relatively cold and less saline Arctic Water (T < 3 °C, S < 35.0; Hopkins (1991)) coming from the Arctic Ocean is brought into the Barents Sea and is carried southward by the East Spitsbergen Current (ESC) and Bear Island Current (BIC) and then flows northward along the western coast of the Svalbard archipelago (Loeng, 1991; Loeng et al., 1997). The water mass carried by ESC and BIC has relatively low salinity and very low temperatures and is often covered by/loaded with seasonal sea ice (Loeng et al., 1997).

Kveithola is a small trough located at the western Barents Sea margin, northwest of Bear Island (Fig. 1). This trough is characterized by water depths ranging from 200 to 400m and is surrounded by Spitsbergenbanken to the north, south, and east (Fig. 1). To the west, Kveithola extends westward and terminates near the continental margin. Two oceanographic processes are currently active in Kveithola. Firstly, Kveithola acts as a pathway for cold and saline bottom waters that are sediment-laden and cascade down from Spitsbergenbanken to the continental slope (Fohrmann et al., 1998). Secondly, the inflow of warm saline Atlantic waters is known to affect Kveithola, as reported by (Rumohr et al., 2001). The bottom currents activities are likely to vary based on the strength of Atlantic water advection, sea-ice distribution, and local oceanographic conditions.

3. Material and methods

3.1. Core collection and CTD

Gravity core OCE2022-KV02-GC (hereafter KV02) was retrieved from the western Barents Sea (74°50.296N, 16°1.3403E, 374 m water depth) during the AREX expedition with R/V *Oceania* in summer 2022 (Fig. 1). The water column temperature and salinity at the coring site were measured in situ by a mini-CTD (conductivity–temperature–depth) profiler at intervals of 1 s. After the sediment core opening, the visual description was performed and color information was obtained based on the Munsell Soil Color Chart. Sediment is mostly light-colored (olive-gray to grayish green) homogenous fine-grained mud and represents continuous sedimentation with no sign of redeposition. The 1.42 m long core was sliced at 1 cm intervals, freeze-dried, and wet sieved through 100 and 500 µm mesh.

Climate
of the Past
Discussions

Table 1. AMS ^{14}C measurements and calibrated ages applying the Marine20 calibration curve. Median ages (in bold) were used for the age-depth model (Fig. 2). Calibrated ages are reported in thousand years before AD 1950 (kyr BP).

Lab ID	Depth (cm)	Dated material	[14]C age	Calibrated age (year BP, 2σ)		
				Min age	Max age	Median age
11617.1.1	3	Mixed benthic foraminifera	2832 ± 81	2396	2658	**2519**
11618.1.1	13	Mixed benthic foraminifera	3795 ± 89	3544	3827	**3684**
11348.1.1	21	Mixed benthic foraminifera	6912 ± 78	7221	7422	**7317**
11619.1.1	39	Mixed benthic foraminifera	7698 ± 123	7926	8219	**8077**
11349.1.1	53	Mixed benthic foraminifera	23722* ± 278		Excluded	
11620.1.1	61	Mixed benthic foraminifera	8199 ± 141	8436	8838	**8647**
11350.1.1	81	Mixed benthic foraminifera	9577 ± 107	10235	10552	**10407**
11621.1.1	111	Mixed benthic foraminifera	14287** ± 236		Excluded	
11350.1.2	130	Mixed benthic foraminifera	12627 ± 143	13990	14530	**14265**
11622.1.1	137	*E. clavatum*	12811 ± 197	14208	14883	**14548**

115   * The radiocarbon age from 53 cm was excluded from the age-depth model (described in section 5.2). ** The radiocarbon age from 111 cm was excluded from the age-depth model (described in section 3.2)

3.2. AMS-^{14}C dates and chronology

The age model for core KV02 is based on eight radiocarbon dates obtained from specimens of

120   the seven mixed benthic foraminifera and one *Elphidium clavatum* sample dated at the MICADAS facility at the Alfred-Wegener Institute in Bremerhaven, Germany (Fig. 2, Table 1). The resulting raw radiocarbon dates were calibrated to calendar ages in the CALIB ^{14}C software (8.2.0; Stuiver et al. (2022)) using the Marine20 dataset (Heaton et al., 2020), and applying a regional radiocarbon reservoir offset (ΔR) of -92 ± 34 years. This ΔR value of −92

125   ± 34 years corresponds to 67 ± 34 years relative to the Marine04 calibration curve based on data from near Bear Island (Mangerud and Gulliksen, 1975). We used http://calib.org/marine/ (last accessed 2024/04/08) to obtain the ΔR value relative to the Marine20 calibration curve. The age obtained in KV02 at 111 cm is older than the age at 130 cm (Table 1). This age reversal was possibly caused by sediment reworking, and the older date was therefore excluded from

130   the age model.

Climate
of the Past
Discussions

3.3.   Foraminiferal analyses

Seventy-six sediment samples from core KV02 were used for foraminiferal analyses. Where possible, a minimum of 300 benthic foraminiferal specimens from the >100 µm fraction of each sample were picked under the light microscope and mounted on faunal slides. However,

135   samples analyzed between 93 and 101 cm had only a few specimens present (less than 15 individuals per sample) and were excluded from the statistical analysis (Fig. 3). The abundance of planktic foraminifera was very low throughout the core (less than 15 individuals per sample), except in the top 45 cm (Fig. 4). Therefore, we excluded these samples with fewer than 15 individuals from the calculation. When necessary, residues were split using a dry microsplitter,

140   and the total number of foraminifera was calculated. The taxonomic classification was performed mostly at the species level, using the generic classification of Loeblich Jr and Tappan (2015).

The total benthic and planktic foraminiferal fluxes were calculated using foraminiferal number

145   (FN) [N g^{-1}], sedimentation accumulation rate (SAR) [cm yr^{-1}], and dry bulk density (DBD) [g cm^{-3}]. The SAR was calculated by using the calibrated ages. The foraminiferal fluxes were calculated by using the following equation (1):

$$\text{Flux (individuals} \times cm^{-2} \times kyr^{-1}) = FN \times DBD \times SAR, \qquad (1)$$

150   ### 3.4.   Stable isotopes and IRD

For stable carbon and oxygen isotope analysis, approximately 20 specimens of the planktic foraminiferal species *Neogloboquadrina pachyderma* and 25 specimens of the benthic species *E. clavatum* were picked from the 100−500 µm size fraction. All samples were cleaned in methanol, and measurements were performed using a Thermo Finnigan MAT 252 mass

155   spectrometer with a Kiel III automatic carbonate preparation device at the Light Stable Isotope Mass Spec Laboratory, Department of Geological Sciences, University of Florida, USA. Measurement precision was better than ±0.04‰ and ±0.02‰ for oxygen and carbon isotopes, respectively.

160   For ice-rafted debris (IRD) content of grains larger than 500 µm were counted in 63 samples. The number of IRD/g dry sediment was calculated. The flux was calculated, using the concentration of IRD [N g^{-1}], SAR, and DBD.
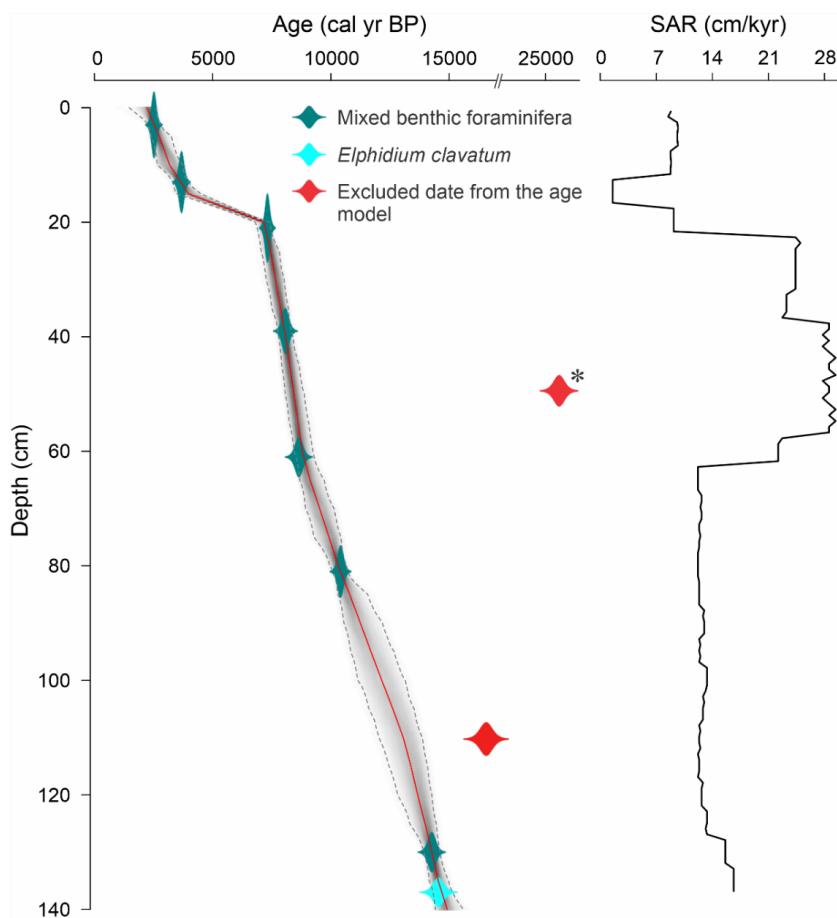
Figure 2: Age-depth model of core OCE2022-KV02-GC. age-depth model and sedimentation accumulation rates (SAR). (The asterisk next to the middle dated layer is described in section 6).

3.5. Organic bulk sediment parameters and biomarker analysis

Total carbon (TC) and total organic carbon (TOC) were measured on homogenized bulk sediment samples using the combustion technique with chromatographic detection, performed with a Thermo Flash 2000 elemental analyzer. The TOC measurements were performed after removing residual carbonate by adding hydrochloric acid. The carbonate content ($CaCO_3$) was calculated according to TOC and TC values, using the following equation (2).

$$CaCO_3 = (TC-TOC) \times 100 \backslash 12 \qquad (2)$$

Lipid biomarkers were analyzed at the Department of Paleoceanography, Institute of Oceanology, Poland, using the procedures described in detail by Krajewska et al. (2023) and Szymczak-Żyła and Lubecki (2022), with some modifications. Freeze-dried samples (~ 4 g),

Climate of the Past
Discussions
EGU Open Access

spiked with surrogate standards (9-octylheptadecene, 7-hexylnonadecane, 2-nonadecanone, and androstanol) were sonication-extracted with a dichloromethane : methanol (2:1 v/v) mixture (3 x 15 ml). After extraction, the raw extracts were concentrated using rotary evaporation and divided into two subsamples (A and B).

Subsample A was fractionated by solid-phase extraction (SPE) using 1% deactivated silica gel. The fraction containing highly branched isoprenoid (IP_{25}) was eluted with a hexane and dichloromethane (1:1 v/v) mixture, whereas the fraction containing alkenones was eluted with dichloromethane. IP_{25} were analyzed using a gas chromatograph coupled to a quadrupole mass spectrometer detector (GCMS-QP2010 Ultra; Shimadzu) according to the procedure described in Krajewska et al. (2023). The concentrations of IP_{25} were calculated based on response factors for IP_{25} and the standards following the procedure described by Belt et al. (2012). Alkenones were analyzed using a gas chromatograph with a flame ionization detector (GC/FID; Nexis GC-2030, Shimadzu) (Krajewska et al., 2023).

To determine the total (free + esterified) polar steroids, subsample B was saponified with 5% KOH in methanol, and then liquid-liquid extraction was carried out in the KOH–methanol extract/chloroform/water system (1/3/2 v/v/v; three times). The combined chloroform fractions were concentrated by rotary evaporation, derivatized to produce the trimethylsilyl derivatives, and analyzed using a gas chromatograph coupled to a mass spectrometer detector (GCMS-QP2010 Ultra; Shimadzu) according to procedure described in Szymczak-Żyła and Lubecki (2022). The analytes were identified based on their retention times and mass spectra and quantified based on response factors derived from daily injections of standard mixtures. The following polar steroids were studied: brassicasterol, campesterol, sitosterol, and dinosterol.

The PIP_{25} indices were calculated by combining IP_{25} with different phytoplankton marker brassicasterol for sea ice reconstruction using equation (3) (Müller et al., 2011).

$$P_pIP_{25} = IP_{25} / (IP_{25} + (p \times c)) \tag{3}$$

where p is the phytoplankton marker concentration (brassicasterol (B)), and c is a balance factor (mean IP_{25} concentration/mean p concentration).

The $U^{K'}_{37}$ index was used to estimate the sea surface temperature (SST). The $U^{K'}_{37}$ index was calculated by the following equation (4) (Bendle and Rosell-Melé, 2004).

$$U^{K'}_{37} = [C_{37:2}]/([C_{37:2}] + [C_{37:3}] + [C_{37:4}]) \tag{4}$$

$U^{K'}_{37}$ values were converted to SSTs using global core-top calibration using equation (5) (Müller

Climate of the Past

Discussions

et al., 1998).

$$U^{K'}_{37} = (0.033 \times SST) + 0.044 \tag{5}$$

210

3.6. X-ray fluorescence spectrometry

X-ray fluorescence (XRF) scanning of the sediment core was conducted at the Department of Paleoceanography, Institute of Oceanology, Poland. An Olympus Vanta M series portable XRF analyzer was used to determine the concentration of the element in the samples. The instrument uses a Rh anode X-ray tube (8-50 kV) as the excitation source. The instrument was operated in Geochem Mode with a scanning time of 45 seconds per beam. The instrument completed one whole scan in 90 seconds by scanning via two beams in sequence. For the interpretation, element ratios, rather than individual elements, are used to prevent closed-sum effects.

4. Results

4.1. Age model

The Bayesian accumulation age-depth modeling program, Bacon 2.4.3 (Blaauw and Christen, 2011) in R statistical software was used to create a suitable age model for sediment core KV02 (Fig. 2). Due to the gravity coring process ~2000 years of sediment have been lost. The calculated sediment accumulation rates (SARs) vary significantly throughout the core. High SARs were observed in the lowermost part of the core, between 138-112 cm of sediment core (between 14.4 and 13.1 kyr BP; 10-15 cm kyr^{-1}), followed by a decrease between 112 and 63 cm (~13 to 8.7 kyr BP; below 10 cm kyr^{-1}). The highest SARs were observed between 62 and 23 cm (~8.7 to 8.1 kyr BP; reaching up to ~30 cm kyr^{-1}), followed by an abrupt decrease of ~1.5 cm kyr^{-1} until 13 cm (up to ~3.4 kyr BP). Then, SARs increased from 13 cm to the surface, reaching ~11 cm kyr^{-1} (Fig. 2).

4.2. Sediment and geochemistry

Between 14.4 and 12.7 kyr BP, coarse content remained low but significantly increased by the end of this interval. From 11.5 to 10.7 kyr BP, the coarse content gradually rose and then stabilized until 9.5 kyr BP. A subsequent gradual increase led to a peak of around 6.8 kyr BP, followed by a notable drop between 8.3 and 8 kyr BP. After 6.8 kyr BP, the coarse content decreased and remained stable until a sudden increase at 3.5 kyr BP (Fig.4). Fe and Ti show fluctuating trends, peaking during the periods of 14.4 - 12.9, 11.7 - 10.9, 10.4 - 9.6, and 9 - 7.5 kyr BP, coinciding with high IRD content (Fig. 4). The TOC percentages remained relatively stable (~1.4 wt%) until ~7.5 kyr BP, with few distinct fluctuations around 11, 9, and 7.5 kyr

BP. After 7.5 kyr BP, the TOC percentage rose noticeably (from 1.15 to 1.8 wt%), and remained constant throughout the rest of the core (Fig. 5).

4.3. Foraminifera

A total of 38 benthic foraminiferal species were identified from the samples counted (33 calcareous and 5 agglutinated). The abundance of agglutinated species was very low; no single species had a relative abundance greater than 1% in any analyzed sample. Selected benthic and planktic foraminiferal species abundances are presented in Fig. 3 and 4 respectively. The benthic foraminiferal concentration varies from a minimum of <1 (three samples at 93, 95, and 101 cm) up to a maximum of 300 specimens g^{-1}.
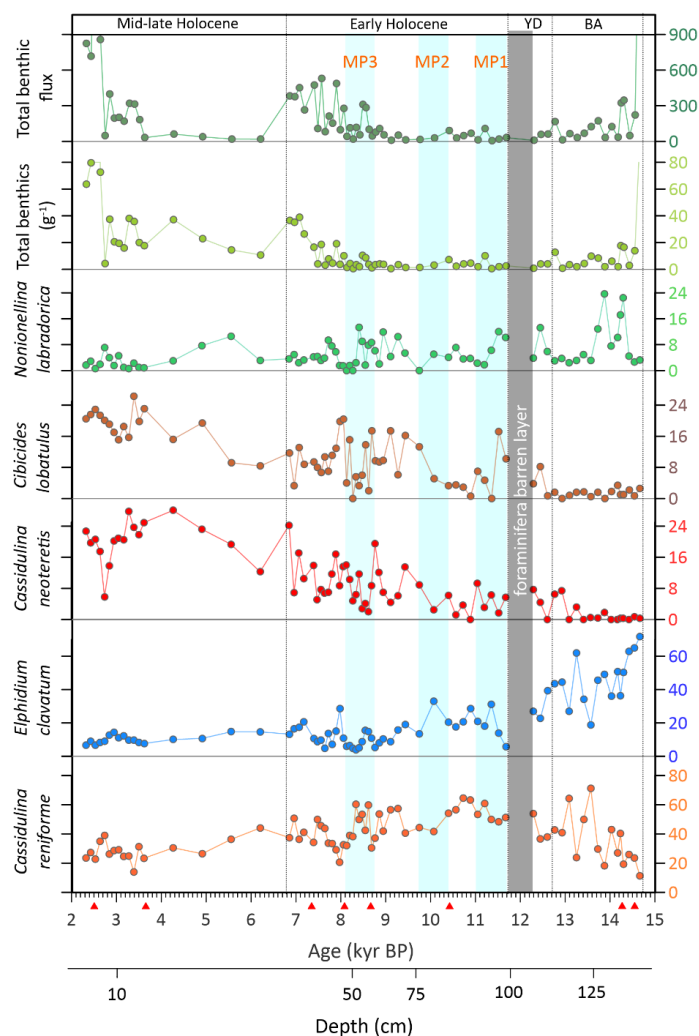
Figure 3: Relative abundances of selected benthic foraminiferal species of core KV02. *Cassidulina reniforme* **(orange line);** *Elphidium clavatum* **(blue line);** *Cassidulina neoteretis* **(red line);** *Cibicides lobatulus* **(brown line);** *Nonionellina labradorica* **(light green line); total benthic foraminiferal concentration and flux (green lines). Blue shadings indicate meltwater pulses. Red triangles next to the bottom x-axis indicate radiocarbon dates. Abbreviations: BA - Bølling-Allerød; YD - Younger Dryas.**

The benthic fauna is dominated by four benthic foraminiferal species; *E. clavatum* (4-72%), *Cassidulina reniforme* (0-71%), *Cassidulina neoteretis* (0-30%), *Cibicides lobatulus* (0-26%) and *Nonionellina labradorica* (0-25%) (Fig. 3). Between 14.4 and ~13 kyr BP, *E. clavatum* and *C. reniforme* dominate the fauna with average values of 47% and 35%, respectively. From 13 to 10.2 kyr BP, *E. clavatum* shows a gradual decreasing trend where the abundance of *C. reniforme* gradually increases. The abundance of *N. labradorica* shows an increasing trend between 12.6 and 11.4 kyr BP. Between 12.1 and 11.8 kyr BP, our record shows very low foraminiferal content. Two species, *C. neoteretis* and *C. lobatulus* show relatively low abundance until 9.5 kyr BP, and from that point abundance increases gradually throughout the records. Similarly, the abundance of *I. norcrossi* gradually increased from 10 kyr BP and reached its maximum abundance between ~9 and 7.5 kyr BP, and then decreased until the end of the record. After 10 kyr BP, both *E. clavatum* and *C. reniforme* decrease gradually until the end of the record.

The polar species *Neogloboquadrina pachyderma* and subpolar *Turborotalita quinqueloba* and *Neogloboquadrina incompta* dominate the planktic foraminiferal assemblages throughout the entire records (Fig. 4). There is a decrease in the abundance of these polar species from ~8 to 7 kyr BP, during which the subpolar species exhibit relatively high abundance. After 7 kyr BP, the polar species dominated the entire record (Fig. 4).

4.4.   Stable isotopes

The benthic foraminiferal $\delta^{18}O$ profile shows highly variable values (+2.7 to +3.6‰) at the base of the core, between 14.7 and 12.5 kyr BP (Fig. 4). Between 12.5 and 8.5 kyr BP, the values are relatively stable with an increase (to positive) around 12.3 and 9 kyr BP. From 9 kyr BP, the $\delta^{18}O$ profile shows highly variable values (+3 to +3.9‰) until 6 kyr BP, with the most depleted value around 8.6 kyr BP (3‰). After 3.5 kyr BP, benthic $\delta^{18}O$ becomes heavier before lightening again around 2.2 kyr BP. Benthic $\delta^{13}C$ values remain generally stable until 11 kyr BP, then become lighter until 8.8 kyr BP (Fig. 5). The $\delta^{13}C$ values are highly variable between 8.8 and 7 kyr BP, with the most depleted value recorded at 8.4 kyr BP. Then, values become

285 more stable before becoming further lighter after 3.5 kyr BP. Planktic $\delta^{18}O$ values vary between
1.90 and 3.02‰.
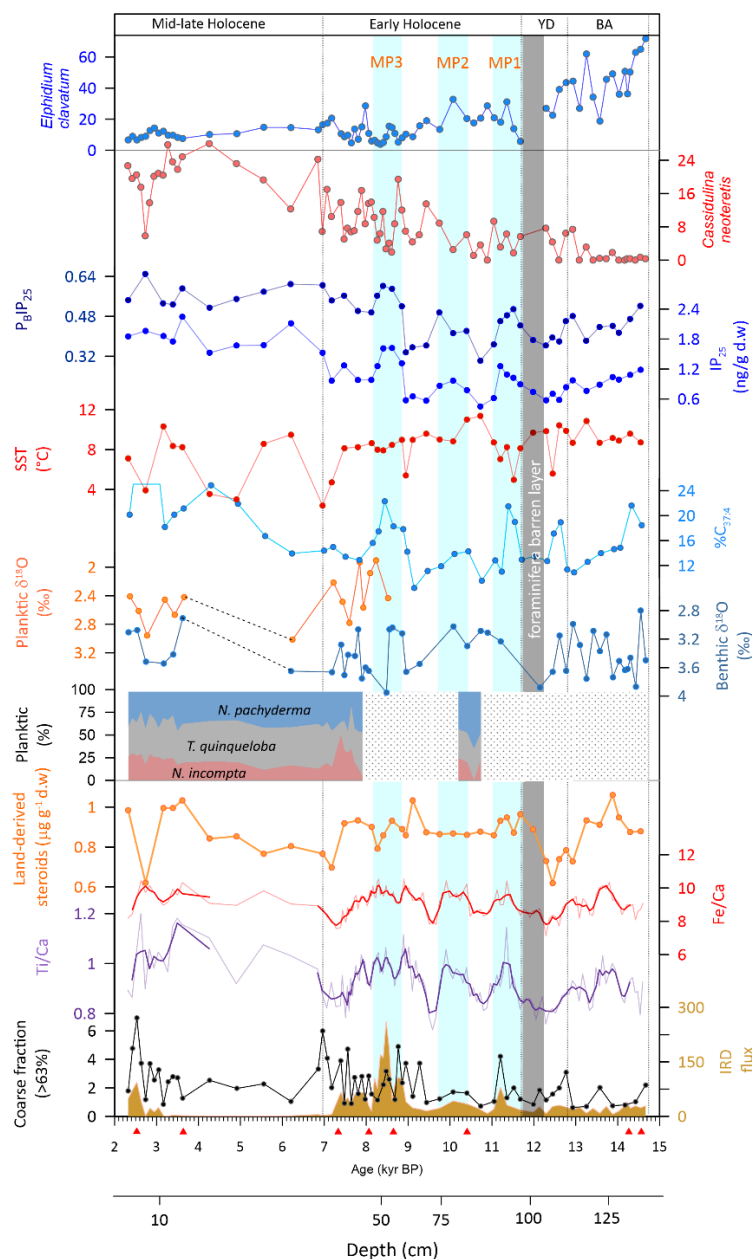
**Figure 4: Combined records of bulk parameters, foraminiferal, and stable oxygen isotope from core KV02.
From bottom to top: IRD content, % of coarse fraction, X-ray fluorescence (XRF) data (thin line = raw**
290 **data, thick line = three-point running average), land-derived steroids (ΣS-land = campesterol + stigmasterol**
+ sitosterol + sitostanol), percentage of planktic foraminifera, benthic and planktic foraminiferal $\delta^{18}O$,

percentage of tetra-unsaturated alkenone (%$C_{37:4}$), alkenone derived SST, concentration of IP_{25}, calculated P_BIP_{25} indices, percentage of *Cassidulina neoteretis*, and percentage of *Elphidium clavatum*. Blue shadings indicate meltwater pulses. Red triangles next to the bottom x-axis indicate radiocarbon dates. Abbreviations: BA - Bølling-Allerød; YD - Younger Dryas.

5.   Discussion

5.1.   Paleoenvironmental evolution during the last 14,700 years

Bølling–Allerød (B-A, ~14.7–12.7 kyr BP) – Initiated with a supply of meltwater

During B-A, the low diversity benthic foraminifera assemblage dominated by *E. clavatum* and *C. reniforme* related to glaciomarine conditions with low temperatures and decreased salinities (Łącka and Zajączkowski, 2016; Hald and Korsun, 1997), possibly caused by an immense supply of meltwater. The high percentage of tetra-unsaturated alkenones (%$C_{37:4}$), an indicator of low temperature and/or low salinity conditions, also suggests meltwater input to our site at the beginning of the interval (Fig. 4) (Bendle et al., 2005; Bard et al., 2000; You et al., 2023). The absence of planktic foraminifera and highly variable, but overall lighter benthic $\delta^{18}O$ also suggest the environment was mostly affected by high meltwater discharge (Fig. 4). There are two possible sources of meltwater to our site. One is from the meltwater plumes triggered by the disintegration of nearby ice sheets [Scandinavian Ice Sheet (SIS) and Svalbard Barents Sea Ice Sheet (SBSIS)] and characterized by fine-grain suspended matter (Leng et al., 2018). The other is melting icebergs, which are characterized by high IRD content. However, the IRD content and coarse clast are low (Fig. 4), therefore, the latter can be ignored and meltwater was supplied to our site by proximal ice sheets. According to Hughes et al. (2016), around 15 kyr BP, both SIS and SBSIS had marine terminates, suggesting that meltwater could have been flowing to the NW Barents Sea from these ice sheets. Alternatively, seasonal sea ice melting could have also contributed to an increased supply of meltwater at our study site. Relatively low IRD deposition and low foraminiferal content indicate increased sedimentation by suspension settling from meltwater plumes (Knies et al., 2007), and possibly the presence of sea ice preventing iceberg drifting (Dowdeswell et al., 2000) reflected in high P_BIP_{25} values (Fig. 4). High Fe/Ca and Ti/Ca values and concentrations of land-derived steroids (ΣS-land) (Fig. 4) indicate enhanced transport of post-glacial terrigenous materials to the NW Barents Sea, likely transported via the meltwater plume (Lantzsch et al., 2017). Therefore, these results demonstrate the importance of suspension-rich meltwater plumes controlling the sedimentation at our site during the B-A interval. Similar turbid meltwater plume-induced sedimentation during the B-A interval has been reported in western Svalbard margins (Rasmussen et al., 2007;

325 Jessen et al., 2010), and NW Barents Sea (Rüther et al., 2012; Lucchi et al., 2013; Melis et al., 2018; Lantzsch et al., 2017) and could be associated with the meltwater pulse 1a (MWP-1a). However, even in the environment affected by turbid meltwater, which could significantly reduce the primary production in the water column by increasing light attenuation, our results indicate some productivity reflected in the high value of phytoplankton biomarkers, relatively

330 high benthic foraminiferal fluxes, and, slightly high and stable TOC (Fig. 5). The supply of terrigenous material from the melting likely supplemented the nutrient levels in the upper surface water mass and boosted surface production (Knies and Stein, 1998).

Initially, a low abundance of *C. neoteretis*, a typical AW indicator (Cage et al., 2021; Jennings

335 et al., 2004; Knudsen et al., 2004) suggests a weak influence from AW current to the study site (Fig. 3). Massive meltwater inflow could have caused a deepening of the halocline (Rasmussen and Thomsen, 2004), hence extending the relatively fresh and cold water to a greater depth. This probably allows warm AW to move further west from our study site.

340 **Younger Dryas (YD, ~12.7–11.7 kyr BP) - Less productive harsh environment**

Our age model suggests that the transition into cold Younger Dryas conditions from the B-A happened around 12.7 kyr BP (Fig. 4). Overall high benthic $\delta^{18}O$ at the initial stage of the YD (~12.7 - 12.3 kyr BP) may reflect more saline bottom water at our site (Fig. 4). This could be attributed to the subsurface AW inflow, as suggested by the presence of *C. neoteretis* (Fig. 4).

345 The high values of %$C_{37:4}$ suggests meltwater input to our site during this interval (Fig. 4). This is also in agreement with findings from studies at the western, southwestern, and northern margins of Svalbard (Bartels et al., 2017; Rasmussen et al., 2007; Ślubowska et al., 2005). Low IP_{25} concentrations (<0.55 ng/g d.w) along with the significantly low phytoplankton biomarker records indicate the presence of extensive sea ice cover at our study site (Fig. 5). This aligns

350 with the finding from the neighboring core located ~30 kilometres to the east (Belt et al., 2015). The IRD content drop after the B-A interval (Fig. 4), and the notable drop of coarse clast content suggests that the primary route of icebergs from the Barents Sea was obstructed by the extended sea ice cover (Forwick and Vorren, 2009).

355 Shortly after the 12.3 kyr BP, several proxies indicated that the NW Barents Sea experienced a very harsh environmental condition that lasted until 11.8 kyr BP. The notable decline of $CaCO_3$ values, relatively low phytoplankton biomarkers, and absence of both planktic and benthic

foraminifera indicate the extreme condition and low primary production (Fig. 5). A comparable

condition, characterized by foraminifera absent layer dated to the early part of the YD, was also

360   observed in a sediment core (recovered from 253 m water depth; core: JM09-020GC; Fig. 1)

from Storfjordrenna by Lacka et al. (2020). They collectively attribute this phenomenon to the

anoxic condition at the bottom. Considering the age uncertainty inherent in the age models, a

similar bottom anoxic condition may exist in NW Barents Sea margins during the YD.

365

15

Climate
of the Past
Discussions
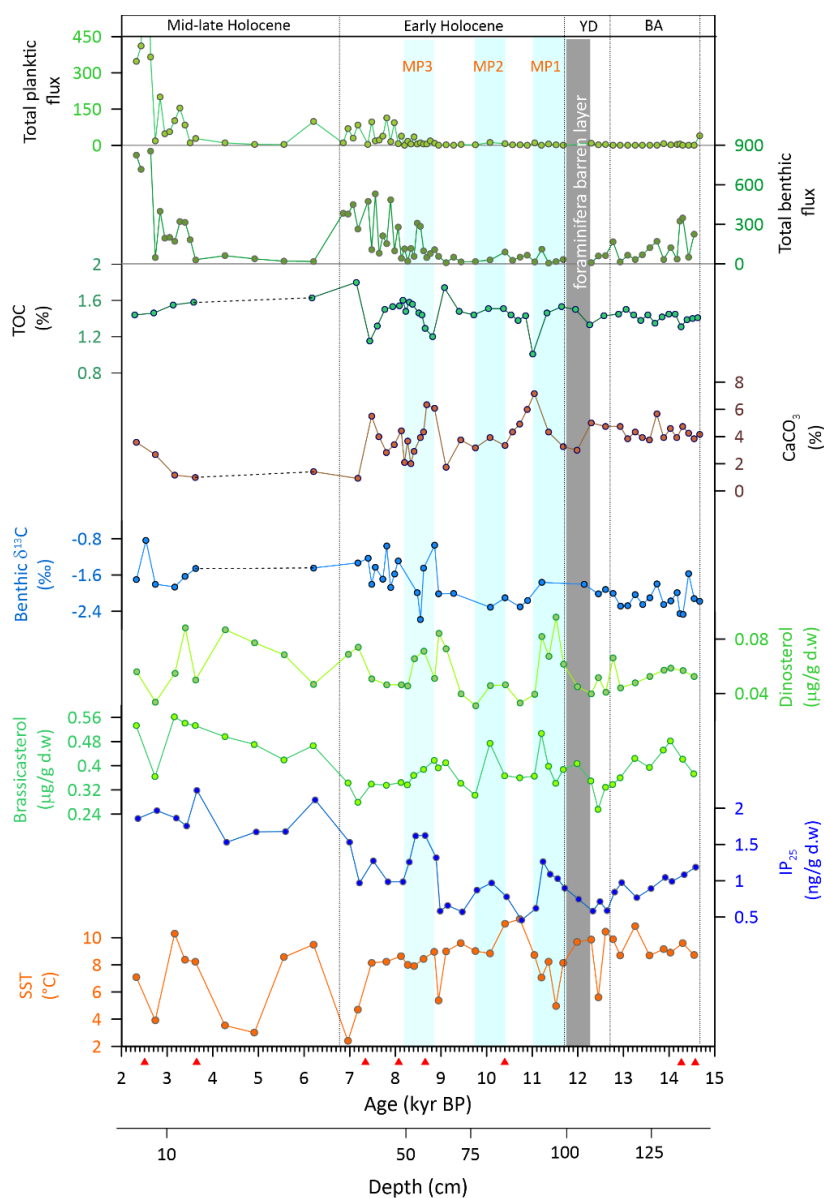
Figure 5: Combined records of bulk parameters, stable carbon isotope, and foraminiferal from core KV02. Bottom to top: alkenone-derived sea surface temperatures (SSTs), IP_{25} concentration, phytoplankton biomarkers (brassicasterol and dinosterol), benthic foraminiferal $\delta^{13}C$, percentage of calcium carbonate, percentage of total organic carbon, total benthic flux and total planktic flux. Blue shadings indicate meltwater pulses. Red triangles next to the bottom x-axis indicate radiocarbon dates. Abbreviations: BA - Bølling-Allerød; YD - Younger Dryas.

Early Holocene (∼11.7–6.8 kyr BP) – Dynamic environment characterized by short cold and warm spells.

Immediately after the YD, a prominent short-lived surface cooling was identified until ~11 kyr BP. The surface was influenced by a cold meltwater plume, as indicated by the increased $\%C_{37:4}$ (Fig. 4; for details see below section 6). This event is also marked by an increase in IP_{25} concentrations, P_BIP_{25} values, and decreased SSTs, altogether reflecting sea ice rafting (Fig. 4). Relatively low abundance of *C. neoteretis* could suggest limited but some influence of AW to our site, possibly as a subsurface water mass below the cold meltwater layer. The high concentrations of phytoplankton biomarkers, increased $CaCO_3$, and TOC suggest high surface productivity, possibly attributed to the freshly exposed terrigenous nutrients, transported via meltwater. The sea surface condition just after YD is also recorded in the records from the southwestern Barents Sea (core PSh-5159N; Risebrobakken et al. (2010)), northwestern Barents Sea (core JM09-KA11-GC; Berben et al. (2014); Belt et al. (2015)), southern Svalbard (core JM09-020GC; Łącka et al. (2015)) and western Svalbard shelf (core HR7-GC; Devendra et al. (2023)), possibly associated with the cold event Preboreal Oscillation. During this period, Arctic water conditions prevailed at most sites, and the Arctic Front was likely situated to the west of the westernmost sites, specifically at the western Barents Sea and Svalbard margin.

Soon after this short cold period, planktic foraminifera appeared for the first time in the records (Fig. 4). The planktic foraminifera fauna was dominated by subpolar *T. quinqueloba* (>40%), occurred around 10.7 kyr BP and persisted until 10.3 kyr BP. A significant increase in subpolar planktic species is also seen in the nearby core M23258 (Sarnthein et al., 2003; Risebrobakken and Berben, 2018) and core JM09-KA11-GC (Berben et al., 2014) since ~10.5 kyr BP. This suggests a short period of warm surface conditions with a low influx of meltwater to the NW Barents Sea, also marked by higher SSTs, and abrupt drop in IP_{25} and P_BIP_{25} (Fig. 4). However, low IP_{25} still indicates the presence of some sea ice, probably seasonal and less extensive than in the preceding interval. This condition was likely common to the region during this interval (Rasmussen and Thomsen, 2015; Berben et al., 2014; Łącka et al., 2015; Devendra et al., 2023;

Belt et al., 2015).

The previous regional studies observed a distinct inflow of warm AW to the SW Svalbard and western Barents Sea margins around ~10 kyr BP (Rasmussen et al., 2007; Rasmussen et al., 2012; Ślubowska-Woldengen et al., 2008; Telesiński et al., 2018; Devendra et al., 2023; Risebrobakken et al., 2011). Similarly, an enhanced influx of AW to our study site was also suggested by increasing abundances of *C. neoteretis* initiated around 9.5 kyr BP (Fig. 3). The increasing abundance of *N. labradorica* observed from 9.3 kyr BP, suggest that the Arctic front was located close to our site (Fig. 3). Risebrobakken and Berben (2018) have also observed similar proximity of the Arctic front to the NW Barents Sea.

Between ~8.8 and 8.2 kyr BP, mild surface cooling associated with a distinct drop in AW influx and an abrupt increase in meltwater influx and sea ice cover reflected by the drop in *C. neoteretis* abundance and an increase in $\%C_{37:4}$ and, IP_{25} and P_BIP_{25} (Fig. 4; see also section 5.2). Subsequently, a slight warming of the surface ensued until 7.3 kyr BP, followed by another short period of pronounced surface cooling around 7 kyr BP, indicated by a drop in SSTs and an increase in IP_{25} records (Fig. 4). A similar pronounced cooling trend around 7 kyr BP has been observed in several other records from the Nordic Seas (Knudsen et al., 2004; Rasmussen et al., 2007; Risebrobakken et al., 2011; Ebbesen et al., 2007; Werner et al., 2013; Werner et al., 2016; Hald et al., 2007).

Mid-Holocene (~6.8–3.5 kyr BP) – Lag deposit associated with strong inflow of Atlantic Water

The interpretation of the interval between 6.8 and 3.5 kyr BP is problematic due to the comparatively low temporal resolution caused by extremely low sedimentation rates (1.5 cm kyr^{-1}; Fig. 5) and, consequently, few data points (n=4). Lag deposit formation on Spitsbergenbanken due to strong winnowing induced by the enhanced influx of AW is likely to be the reason for this low sedimentation at our site corroborated by the previous studies (Vorren et al., 1984; Elverhøi and Henrich, 2002; Lantzsch et al., 2017). Following the trend from the latter part of the previous time interval, an enhanced influx of AW is indicated by the continuously increasing presence of *C. neoteretis* (Fig. 3). Planktic foraminifera fauna was dominated by subpolar *T. quinqueloba* (>40%) suggesting relatively warm surface conditions (Fig. 4). Support for similar warmer surface conditions after 7 kyr BP was also observed in SW Barents Sea (Risebrobakken and Berben, 2018) and the western Barents Sea (Berben et al., 2014). However, signs of sea ice expansion and fresher surface condition were suggested by

Climate
of the Past
Discussions

435   the increased IP_{25} and P_BIP_{25}, and elevated $\%C_{37:4}$ (Fig. 4). This suggests an inflow of AW
        flowing beneath this fresher surface water layer. A similar oceanographic condition with
        subsurface AW influx during the mid-Holocene has also been observed further north of the
        region (core: HR7-GC; Fig. 1) (Devendra et al., 2023). This may indicate that the Arctic front
        is located along the margin southwards from Svalbard, close to our study site, and is in
440   agreement with Risebrobakken and Berben (2018).

**Late Holocene (after ~3.5 kyr BP) – Amelioration of the bottom environment by strong
currents**

        A drop in *N. pachyderma* abundance (~15%) and an increase in abundance of subpolar planktic
445   species indicate that the surface water was characterized by relatively warm conditions (Fig. 4).
        Abrupt drop (to positive) in both benthic and planktic $\delta^{18}O$ records (Fig. 4) potentially due to
        the AW expansion over the entire water column. High P_BIP_{25} (>0.5) values, along with the
        presence of IP_{25}, indicate a marginal sea ice zone or seasonal ice cover at our site (Fig. 4). These
        conditions with marginal sea ice significantly increased the annual productivity, which is
450   reflected in high foraminiferal fluxes, $CaCO_3$, TOC, phytoplankton biomarkers, and lighter
        benthic $\delta^{13}C$ (Fig. 5).

        This interval is also characterized by an increase in the content of coarse sediment at Kveithola
        (Fig. 4). Similar late Holocene coarser bottom conditions were identified from
        Spitsbergenbanken due to winnowing enhanced by bottom currents (Devendra et al., 2023;
455   Andruleit et al., 1996). According to Sarnthein et al. (2003), pulsed inflows of AW to the
        western Barents Sea occurred after ~3 kyr BP, a timing that coincides with other observations
        in Fram Strait (Müller et al., 2012), western Svalbard (Devendra et al., 2023), eastern Svalbard
        (Pawłowska et al., 2020), and the SW Barents Sea (core PSh-5159N) (Risebrobakken et al.,
        2010). A significantly high abundance of *C. neoteretis* in our records also suggests an influx of
460   AW to our site. Simultaneously, the high abundance of *C. lobatulus* that typically prefers high-
        energy environments with bottom currents (Wollenburg and Mackensen, 1998; Hald and
        Korsun, 1997; Mackensen et al., 1995) indicates that the AW current significantly influenced
        the environment. Therefore, we suggest that strengthening AW inflow and active bottom
        current-induced erosive conditions would have promoted the bottom coarsening condition
465   within the region.

        Alternatively, the coarsening could also be affected by both biogenic and terrigenous particle

Climate of the Past
Discussions

influx (Lantzsch et al., 2017). The increase in biogenic carbonate content during this interval is

470 reflected in high $CaCO_3$ content in our records (Fig. 5), which could be related to AW-induced high surface water productivity, led to a decrease in terrigenous materials supply (Lantzsch et al., 2017) to our site. Our records show a decrease in terrigenous signals reflected in decreasing terrigenous biomarker and Fe/Ca (Fig. 4). Therefore, we suggest that the coarser sediment accumulation within the region would have been promoted by the combined effect of increased biogenic export from high surface annual productivity, and strengthening of AW inflow and

475 active bottom current induced erosive conditions.

5.2. Early Holocene meltwater outbursts to the western Barents Sea

We use the $\%C_{37:4}$ as an indicator of meltwater pulses at our study site. $\%C_{37:4}$ values are highly variable during the early Holocene, however, we observed three distinct increases in $\%C_{37:4}$

480 values (Fig. 6) that likely correspond to meltwater pulses (MP). We named these pulses MP1, MP2, and MP3, which occurred around 11.7–11 kyr BP, 10.4–9.7 kyr BP, and 8.8–8.2 kyr BP, respectively (Fig. 6). The absence of planktic foraminifera during these meltwater pulses may also support reduced salinity and turbid conditions in the surface water layer due to this turbid meltwater discharge (Fig. 4).

485

The occurrence of meltwater pulses was associated with preceding surface warming in the western Barents Sea (Fig. 6). The early Holocene meltwater pulses into the western Barents Sea were most likely controlled by different meltwater sources, such as 1) discharge from the disintegrating ice sheet from the northern part of Spitsbergenbanken to the inner Storfjorden, 2)

490 the meltwater outburst from paleo Ice Lakes, and 3) meltwater from the sea ice melting during the summer. These meltwater pulses were also marked by an abrupt increase in sea ice content (higher IP_{25} values), a decrease in SSTs, and sluggish AW influx to the NW Barents Sea seen as the lower abundance of *C. neoteretis* and lighter benthic $\delta^{18}O$ (Fig. 6).

495 **MP1** is characterized by peaks in IRD content, land-derived steroids (ΣS-land), coarse clast content, and an increased Ti/Ca and Fe/Ca suggest an elevated supply of terrigenous materials, possibly transported by sediment-laden meltwater and icebergs and/or sea ice (Fig. 4). The observation of increased ice rafting in the study site coincides with higher IRD content in the NW Barents Sea (Lantzsch et al., 2017) and Storfjorden around 11.5 kyr BP (Rasmussen et al.,

500 2007). High drift sediment deposition from a disintegrating ice sheet from the northern part of

Spitsbergenbanken was found in Kveithola (Rüther et al., 2012), indicating that meltwater from an ice sheet from the northern part of Spitsbergenbanken flowed to Kveithola. Moreover, evidence of meltwater influence, as recorded in cores HR7-GC and JM09-020GC on the southern Svalbard shelf, supports the statement that the meltwater prominently originated from the disintegrating ice sheet. The timing of this event compares well with the final retreat of the glaciers over the Svalbard and Barents Sea (Svendsen et al., 1996; Hughes et al., 2016). Alternatively, the outburst of Baltic Ice Lake to the North Sea (Fig.7a) around 11.5 kyr BP (Bjorck, 1995; Bodén et al., 1997; Nesje et al., 2004; Jakobsson et al., 2007), may have also contributed substantially to the development of MP1, considering the drainage timing. Hence, we propose that the formation of MP1 is primarily attributed to the combined influence of meltwater discharge from ice sheets and drainage from Baltic Ice Lake. However, further research is required to understand and track the meltwater signals from the Baltic Lake outburst to the western Barents Sea.

MP2, which occurred between 10.4–9.7 kyr BP, is associated with lower volumes of meltwater influx or distribution to our study site compared to MP1. This is reflected in the relatively lower %$C_{37:4}$ during the MP2 than in the MP1 (Fig. 6), suggesting that at least one of the meltwater sources for the MP1 may have partially or completely stopped during the MP2. The meltwater originating from the northern part of Spitsbergenbanken likely partially or completely stopped, supported by a significant reduction of meltwater influence on the southern Svalbard shelf (core HR07-GC; Devendra et al., 2023). After ~10.5 kyr BP, while the remnants of the last glacial ice sheet had retreated beyond the coastline of Norway, large parts of Fennoscandia remained covered by ice (Hughes et al., 2016). The orbital forced summer insolation was also high during this period (Laskar et al., 2004) (Fig. 6), which could promote the melting of the remaining ice sheet and sea ice during the summer and meltwater release to the Barents Sea. Moreover, drainage from the Ancylus Lake (Fig. 7b) to the North Sea was also observed between 10.4 and 9.2 kyr BP (Bjorck, 1995; Nesje et al., 2004), and could have been transported to the western Barents Sea. Therefore, a substantial amount of turbid meltwater (reflected in higher Ti/Ca and Fe/Ca, and land-derived steroids; Figs. 4 and 6) could be transported to the western Barents Sea due to the deglaciation process and possibly by the lake outburst flood.
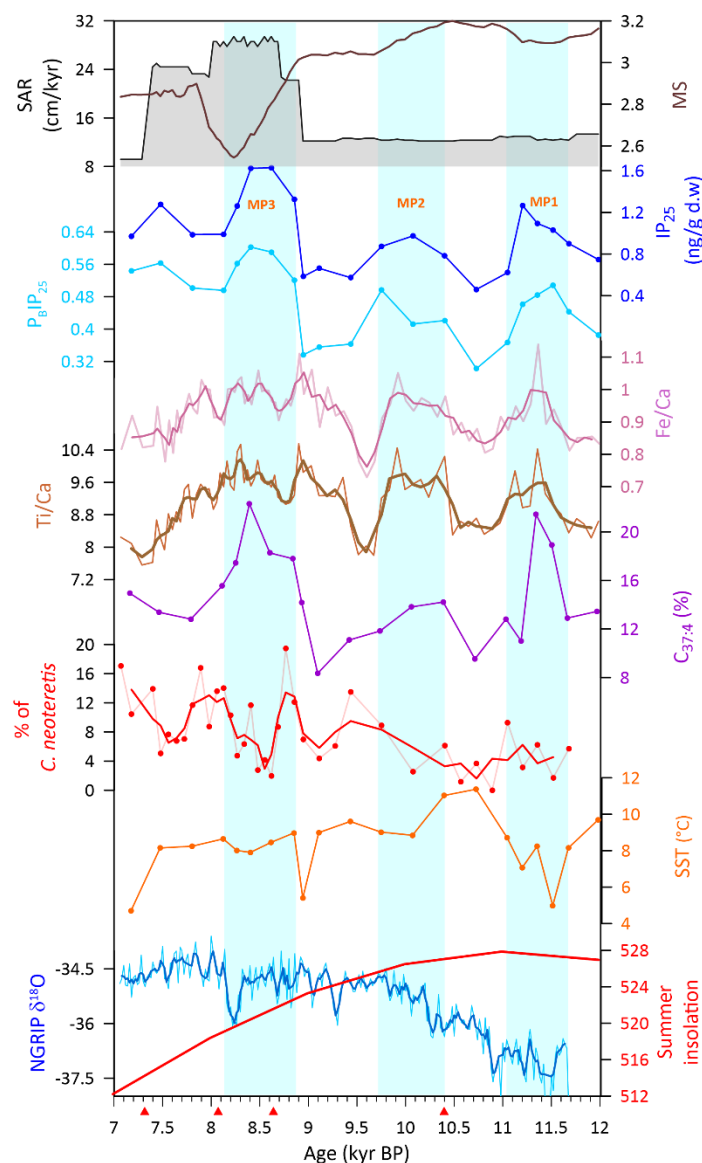
Figure 6: Proxy records of early Holocene meltwater events. From bottom to top: δ18O of the NGRIP core (black line) (Grootes and Stuiver, 1997) **and summer insolation at 77°N (red line)** (Laskar et al., 2004),
535 **alkenone-derived SST, percentage of *Cassidulina neoteretis*, percentage of tetra-unsaturated alkenone (%C37:4), Ti/Ca and Fe/Ca, calculated PBIP25 indices, concentration of IP25, sediment accumulation rate (SAR) and magnetic susceptibility. Blue shadings indicate meltwater pulses (MP1, MP2, and MP3). Red triangles next to the x-axis indicate radiocarbon dates.**

540 **MP3** occurred between ~8.8 and 8.2 kyr BP, likely coinciding with an 8.2 kyr BP cold event (Barber et al., 1999; Johnsen et al., 2001; Von Grafenstein et al., 1998). Since all the marine

Climate
of the Past
Discussions

terminates glaciers around Svalbard were retreated to terrestrial margins and coasts remained ice-free through this interval e.g., (Farnsworth et al., 2020), the source of this meltwater is likely from the seasonal sea ice melting. The coincidence of low benthic carbon isotope values with this

545 meltwater pulse is consistent with developing a low-salinity surface layer that would increase stratification and inhibit ventilation (Fig. 5).
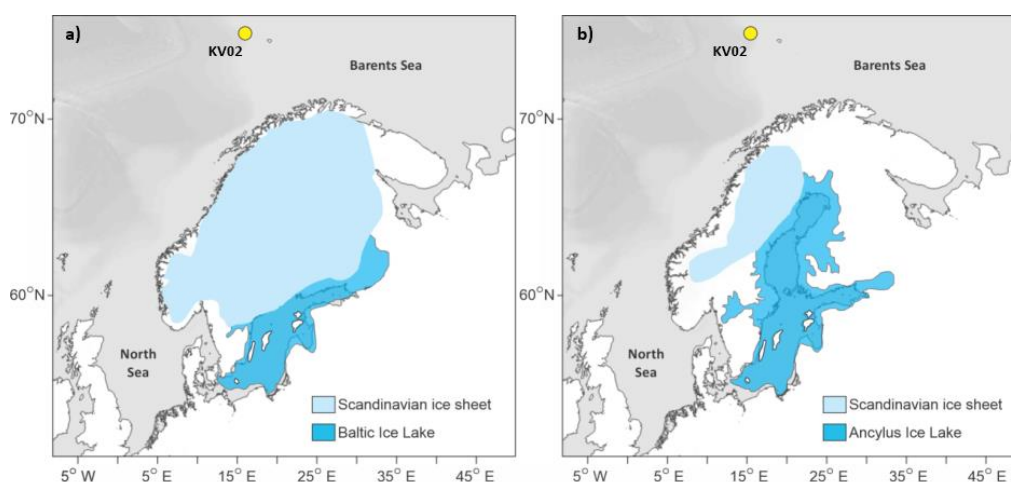
Figure 7: The locations of the Scandinavian Ice Sheet (modified from Hughes et al. (2016)) extent and Paleo
550 **Ice Lakes (modified from Harrison et al. (2018)). a) Baltic Ice Lake around 11.5 ka and b) Ancylus Ice Lake**
around 10 ka in present-day Fenno-Scandinavia. The yellow dots indicate the sediment core KV02.

In addition to sea ice melting, turbid freshwater associated with high terrestrial materials could be transported from the Norwegian Sea via Storegga tsunami currents triggered by the Storegga

555 slide that occurred around 8.2 kyr BP in the Norwegian Sea (Fig. 1a). Within the Norwegian Sea, this turbid water, characterized by its freshness and abundance of terrestrial materials, may be further influenced by tsunami backwash (Bondevik et al., 2012). Rüther et al. (2012) speculate that the Storegga Tsunami currents may also have affected the NW Barents Sea. The computer simulation suggests that strong flow velocity generated by tsunami currents could

560 reach and disturb the sediment up to 74 °N (Bondevik et al., 2024). The abrupt decrease in magnetic susceptibility through this part of the record (supplementary Fig. 1) would suggest a sudden change in the sediment transport to the area. A high sediment accumulation (Fig. 6) during this interval, also a significant drop in sand content, and an increase in fine-grained sediment (supplementary Fig. 1) suggest that sediment suspension would play a vital role in

565 sedimentation at Kveithola. An age reversal (marked by an asterisk in Fig. 2) between the two

radiocarbon-dated layers (8.07 and 8.65 kyr BP), potentially due to sediment reworking and redeposit of the older foraminiferal shells to our site. This could be related to Storegga slide-induced current influence on the western Barents Sea reported by Rüther et al. (2012). Unfortunately, the exact timing of the influence of Storegga tsunami currents on the Kveithola 570 cannot be determined in our records due to the limited number of radiocarbon dates in this interval. Nevertheless, changes in the sedimentary environment during this interval (Fig. 6 and supplementary Fig. 1), consistent with the Storegga tsunami records in the region, lead us to conclude the NW Barents Sea could have also been affected by the tsunami currents, which brought meltwater to the NW Barents Sea.

575

6.   Conclusions

The multiproxy reconstruction using a sediment core from the northwest Barents Sea, representing the last 14,700 years, shows variations in water mass properties and sea surface features. We identified four sediment-laden meltwater pulses to the western Barents Sea 580 between 14,700 and 8,200 cal years BP. These meltwater events are characterized by sudden drops in sea surface temperatures, increased sea ice formation and terrigenous supply, and limited influence of Atlantic Water on the northwestern Barents Sea. The impact of the Storegga tsunami, which occurred around the 8,200 cal years BP cooling event is likely to have redistributed the sediment in Kveithola. Furthermore, the observed coarsening of the 585 northwestern Barents shelf after 3,500 cal years BP and a dynamic environment characterized by increased Atlantic Water influx demonstrate the complex interaction of processes shaping the region's environmental evolution. Overall, our findings advance our knowledge of the last deglaciation in the northwest Barents Sea and have implications for future studies into climate change and the reconstruction of the paleoenvironment in this region.

590

Author contributions. DD, NS, MMT, and MZ collected the sediment core. DD and MZ designed the research and experiments. DD constructed the age-depth model. DD, NS, MŁ, MS-Ż, and MK performed the formal analysis. DD wrote the original manuscript draft. All authors contributed to data interpretation, writing, and editing of the final manuscript.

595

Climate
of the Past
Discussions

References

Ackermann, L., Danek, C., Gierz, P., and Lohmann, G.: AMOC Recovery in a multicentennial scenario using a coupled atmosphere-ocean-ice sheet model, Geophysical Research Letters, 47, e2019GL086810, 2020.

Alsos, I. G., Rijal, D. P., Ehrich, D., Karger, D. N., Yoccoz, N. G., Heintzman, P. D., Brown, A. G., Lammers, Y., Pellissier, L., Alm, T., Brathen, K. A., Coissac, E., Merkel, M. K. F., Alberti, A., Denoeud, F., Bakke, J., and PhyloNorway, C.: Postglacial species arrival and diversity buildup of northern ecosystems took millennia, Science Advances, 8, eabo7434, 10.1126/sciadv.abo7434, 2022.

Andruleit, H., Freiwald, A., and Schäfer, P.: Bioclastic carbonate sediments on the southwestern Svalbard shelf, Marine Geology, 134, 163-182, 10.1016/0025-3227(96)00044-8, 1996.

Barber, D. C., Dyke, A., Hillaire-Marcel, C., Jennings, A. E., Andrews, J. T., Kerwin, M. W., Bilodeau, G., McNeely, R., Southon, J., and Morehead, M. D. J. N.: Forcing of the cold event of 8,200 years ago by catastrophic drainage of Laurentide lakes, 400, 344-348, 1999.

Bard, E., Rostek, F., Turon, J. L., and Gendreau, S.: Hydrological impact of heinrich events in the subtropical northeast atlantic, Science, 289, 1321-1324, 10.1126/science.289.5483.1321, 2000.

Bartels, M., Titschack, J., Fahl, K., Stein, R., Seidenkrantz, M.-S., Hillaire-Marcel, C., and Hebbeln, D.: Atlantic Water advection vs. glacier dynamics in northern Spitsbergen since early deglaciation, Climate of the Past, 13, 1717-1749, 10.5194/cp-13-1717-2017, 2017.

Belt, S. T., Brown, T. A., Rodriguez, A. N., Sanz, P. C., Tonkin, A., and Ingle, R.: A reproducible method for the extraction, identification and quantification of the Arctic sea ice proxy IP 25 from marine sediments, Analytical methods, 4, 705-713, 2012.

Belt, S. T., Cabedo-Sanz, P., Smik, L., Navarro-Rodriguez, A., Berben, S. M. P., Knies, J., and Husum, K.: Identification of paleo Arctic winter sea ice limits and the marginal ice zone: Optimised biomarker-based reconstructions of late Quaternary Arctic sea ice, Earth and Planetary Science Letters, 431, 127-139, 10.1016/j.epsl.2015.09.020, 2015.

Bendle, J. and Rosell-Melé, A.: Distributions of UK37 and UK37′ in the surface waters and sediments of the Nordic Seas: Implications for paleoceanography, Geochemistry, Geophysics, Geosystems, 5, Q11013, 10.1029/2004gc000741, 2004.

Bendle, J., Rosell-Melé, A., and Ziveri, P.: Variability of unusual distributions of alkenones in the surface waters of the Nordic seas Paleoceanography, 20, PA2001, https://doi.org/10.1029/2004PA001025, 2005.

Berben, S. M. P., Husum, K., Cabedo-Sanz, P., and Belt, S. T.: Holocene sub-centennial evolution of Atlantic water inflow and sea ice distribution in the western Barents Sea, Climate of the Past, 10, 181-198, 10.5194/cp-10-181-2014, 2014.

Bjarnadóttir, L. R., Rüther, D. C., Winsborrow, M. C. M., and Andreassen, K.: Grounding-line dynamics during the last deglaciation of Kveithola, W Barents Sea, as revealed by seabed geomorphology and shallow seismic stratigraphy, Boreas, 42, 84-107, 10.1111/j.1502-3885.2012.00273.x, 2012.

Bjorck, S.: A Review of the History of the Baltic Sea, 13.0-8.0 Ka Bp, Quaternary International, 27, 19-40, Doi 10.1016/1040-6182(94)00057-C, 1995.

Blaauw, M. and Christen, J. A.: Flexible paleoclimate age-depth models using an autoregressive gamma process, Bayesian Analysis, 6, 10.1214/11-ba618, 2011.

Bodén, P., Fairbanks, R. G., Wright, J. D., and Burckle, L. H.: High-resolution stable isotope records from southwest Sweden: the drainage of the Baltic Ice Lake and Younger Dryas Ice Margin Oscillations, Paleoceanography, 12, 39-49, 1997.

Bondevik, S., Stormo, S. K., and Skjerdal, G.: Green mosses date the Storegga tsunami to the chilliest decades of the 8.2 ka cold event, Quaternary Science Reviews, 45, 1-6, 10.1016/j.quascirev.2012.04.020, 2012.

Bondevik, S., Risebrobakken, B., Gibbons, S. J., Rasmussen, T. L., and Lovholt, F.: Contamination of 8.2 ka cold climate records by the Storegga tsunami in the Nordic Seas, Nat Commun, 15, 2904, 10.1038/s41467-024-47347-9, 2024.

Bondevik, S., Løvholt, F., Harbitz, C., Mangerud, J., Dawson, A., and Inge Svendsen, J.: The Storegga Slide tsunami—comparing field observations with numerical simulations, Marine and Petroleum Geology, 22, 195-208, 10.1016/j.marpetgeo.2004.10.003, 2005.

Cage, A. G., Pieńkowski, A. J., Jennings, A., Knudsen, K. L., and Seidenkrantz, M.-S.: Comparative analysis of six common foraminiferal species of the genera Cassidulina , Paracassidulina , and Islandiella from the Arctic–North Atlantic domain, Journal of Micropalaeontology, 40, 37-60, 10.5194/jm-40-37-2021, 2021.

Devendra, D., Łącka, M., Szymańska, N., Szymczak-Żyła, M., Krajewska, M., Weiner, A. K. M., De Schepper, S., Simon, M. H., and Zajączkowski, M.: The development of ocean currents and the response of the cryosphere on the Southwest Svalbard shelf over the Holocene, Global and Planetary Change, 228, 104213, 10.1016/j.gloplacha.2023.104213, 2023.

Dowdeswell, Whittington, Jennings, Andrews, Mackensen, and Marienfeld: An origin for laminated glacimarine sediments through sea-ice build-up and suppressed iceberg rafting, Sedimentology, 47, 557-576, 10.1046/j.1365-3091.2000.00306.x, 2000.

Ebbesen, H., Hald, M., and Eplet, T. H.: Lateglacial and early Holocene climatic oscillations on the western Svalbard margin, European Arctic, Quaternary Science Reviews, 26, 1999-2011, 10.1016/j.quascirev.2006.07.020, 2007.

Elverhøi, A. and Henrich, R.: Past glaciomarine environments, in: Modern and Past Glacial Environments, Elsevier, 391-415, 2002.

Farnsworth, W. R., Allaart, L., Ingólfsson, Ó., Alexanderson, H., Forwick, M., Noormets, R., Retelle, M., and Schomacker, A.: Holocene glacial history of Svalbard: Status, perspectives and challenges, Earth-Science Reviews, 208, 10.1016/j.earscirev.2020.103249, 2020.

Fohrmann, H., Backhaus, J. O., Blaume, F., and Rumohr, J.: Sediments in bottom-arrested gravity plumes: Numerical case studies, Journal of Physical Oceanography, 28, 2250-2274, 1998.

Forwick, M. and Vorren, T. O.: Late Weichselian and Holocene sedimentary environments and ice rafting in Isfjorden, Spitsbergen, Palaeogeography, Palaeoclimatology, Palaeoecology, 280, 258-274, 10.1016/j.palaeo.2009.06.026, 2009.

Groot, D. E., Aagaard-Sørensen, S., and Husum, K.: Reconstruction of Atlantic water variability during the Holocene in the western Barents Sea, Climate of the Past, 10, 51-62, 10.5194/cp-10-51-2014, 2014.

Grootes, P. and Stuiver, M.: Oxygen 18/16 variability in Greenland snow and ice with 10^{-3}-to 10^5-year time resolution, Journal of Geophysical Research: Oceans, 102, 26455-26470, 1997.

Hald, M. and Korsun, S.: Distribution of modern benthic foraminifera from fjords of Svalbard, European Arctic, The Journal of Foraminiferal Research, 27, 101-122, 1997.

Hald, M., Andersson, C., Ebbesen, H., Jansen, E., Klitgaard-Kristensen, D., Risebrobakken, B., Salomonsen, G. R., Sarnthein, M., Sejrup, H. P., and Telford, R. J.: Variations in temperature and extent of Atlantic Water in the northern North Atlantic during the Holocene, Quaternary Science Reviews, 26, 3423-3440, 10.1016/j.quascirev.2007.10.005, 2007.

Harrison, S., Smith, D. E., and Glasser, N. F.: Late Quaternary meltwater pulses and sea level change, Journal of Quaternary Science, 34, 1-15, 10.1002/jqs.3070, 2018.

Heaton, T. J., Köhler, P., Butzin, M., Bard, E., Reimer, R. W., Austin, W. E. N., Bronk Ramsey, C., Grootes, P. M., Hughen, K. A., Kromer, B., Reimer, P. J., Adkins, J., Burke, A., Cook, M. S., Olsen, J., and Skinner, L. C.: Marine20—The Marine Radiocarbon Age Calibration Curve (0–55,000 cal BP), Radiocarbon, 62, 779-820, 10.1017/rdc.2020.68, 2020.

Hopkins, T. S.: The GIN Sea—A synthesis of its physical oceanography and literature review 1972–1985, Earth-Science Reviews, 30, 175-318, 10.1016/0012-8252(91)90001-v, 1991.

Hughes, A. L. C., Gyllencreutz, R., Lohne, Ø. S., Mangerud, J., and Svendsen, J. I.: The last Eurasian ice sheets – a chronological database and time-slice reconstruction, DATED-1, Boreas, 45, 1-45, 10.1111/bor.12142, 2016.

Jakobsson, M., Björck, S., Alm, G., Andrén, T., Lindeberg, G., and Svensson, N.-O.: Reconstructing the Younger Dryas ice dammed lake in the Baltic Basin: Bathymetry, area and volume, Global and Planetary Change, 57, 355-370, 10.1016/j.gloplacha.2007.01.006, 2007.

Jennings, A. E., Weiner, N. J., Helgadottir, G., and Andrews, J. T.: Modern foraminiferal faunas of the southwestern to northern Iceland shelf: Oceanographic and environmental controls, J Foramin Res, 34, 180-207, Doi 10.2113/34.3.180, 2004.

Jessen, S. P., Rasmussen, T. L., Nielsen, T., and Solheim, A.: A new Late Weichselian and Holocene marine chronology for the western Svalbard slope 30,000–0 cal years BP, Quaternary Science Reviews, 29, 1301-1312, 10.1016/j.quascirev.2010.02.020, 2010.

Johnsen, S. J., Dahl-Jensen, D., Gundestrup, N., Steffensen, J. P., Clausen, H. B., Miller, H., Masson-Delmotte, V., Sveinbjörnsdottir, A. E., and White, J.: Oxygen isotope and palaeotemperature records from six Greenland ice-core stations: Camp Century, Dye-3, GRIP, GISP2, Renland and NorthGRIP, Journal of Quaternary Science: Published for the Quaternary Research Association, 16, 299-307, 2001.

715 Knies, J. and Stein, R.: New aspects of organic carbon deposition and its paleoceanographic implications along the Northern Barents Sea Margin during the last 30,000 years, Paleoceanography, 13, 384-394, 10.1029/98pa01501, 1998.

Knies, J., Vogt, C., Matthiessen, J., Nam, S.-I., Ottesen, D., Rise, L., Bargel, T., and Eilertsen, R. S.: Re-advance of the Fennoscandian Ice Sheet during Heinrich Event 1, Marine Geology, 240, 1-18, 720 10.1016/j.margeo.2007.01.006, 2007.

Knudsen, K. L., Jiang, H., Jansen, E., Eiríksson, J., Heinemeier, J., and Seidenkrantz, M. S.: Environmental changes off North Iceland during the deglaciation and the Holocene: foraminifera, diatoms and stable isotopes, Marine Micropaleontology, 50, 273-305, 10.1016/s0377-8398(03)00075-6, 2004.

Krajewska, M., Lubecki, L., and Szymczak-Żyła, M.: Sources of sedimentary organic matter in Arctic fjords: 725 Evidence from lipid molecular markers, Continental Shelf Research, 264, 105053, 10.1016/j.csr.2023.105053, 2023.

Lacka, M., Michalska, D., Pawlowska, J., Szymanska, N., Szczucinski, W., Forwick, M., and Zajaczkowski, M.: Multiproxy paleoceanographic study from the western Barents Sea reveals dramatic Younger Dryas onset followed by oscillatory warming trend, Sci Rep, 10, 15667, 10.1038/s41598-020-72747-4, 2020.

730 Łącka, M. and Zajączkowski, M.: Does the recent pool of benthic foraminiferal tests in fjordic surface sediments reflect interannual environmental changes? The resolution limit of the foraminiferal record, Annales Societatis Geologorum Poloniae, 86, 59–71, 10.14241/asgp.2015.019, 2016.

Łącka, M., Zajączkowski, M., Forwick, M., and Szczuciński, W.: Late Weichselian and Holocene palaeoceanography of Storfjordrenna, southern Svalbard, Climate of the Past, 11, 587-603, 10.5194/cp-11-587- 735 2015, 2015.

Lantzsch, H., Hanebuth, T. J. J., Horry, J., Grave, M., Rebesco, M., and Schwenk, T.: Deglacial to Holocene history of ice-sheet retreat and bottom current strength on the western Barents Sea shelf, Quaternary Science Reviews, 173, 40-57, 10.1016/j.quascirev.2017.08.016, 2017.

Laskar, J., Robutel, P., Joutel, F., Gastineau, M., Correia, A. C., and Levrard, B.: A long-term numerical solution 740 for the insolation quantities of the Earth, Astronomy & Astrophysics, 428, 261-285, 2004.

Leng, W., von Dobeneck, T., Bergmann, F., Just, J., Mulitza, S., Chiessi, C. M., St-Onge, G., and Piper, D. J.: Sedimentary and rock magnetic signatures and event scenarios of deglacial outburst floods from the Laurentian Channel Ice Stream, Quaternary Science Reviews, 186, 27-46, 2018.

Li, Q., Marshall, J., Rye, C. D., Romanou, A., Rind, D., and Kelley, M.: Global climate impacts of Greenland and 745 Antarctic meltwater: A comparative study, Journal of Climate, 36, 3571-3590, 2023.

Loeblich Jr, A. R. and Tappan, H.: Foraminiferal genera and their classification, Springer2015.

Loeng, H.: Features of the Physical Oceanographic Conditions of the Barents Sea, Polar Research, 10, 5-18, DOI 10.1111/j.1751-8369.1991.tb00630.x, 1991.

Loeng, H., Ozhigin, V., and Adlandsvik, B.: Water fluxes through the Barents Sea, Ices Journal of Marine Science, 750 54, 310-317, DOI 10.1006/jmsc.1996.0165, 1997.

Lohmann, J. and Ditlevsen, P. D.: Risk of tipping the overturning circulation due to increasing rates of ice melt, Proceedings of the National Academy of Sciences, 118, e2017989118, 2021.

Lucchi, R. G., Sagnotti, L., Camerlenghi, A., Macrì, P., Rebesco, M., Pedrosa, M. T., and Giorgetti, G.: Marine sedimentary record of Meltwater Pulse 1a along the NW Barents Sea continental margin, arktos, 1, 10.1007/s41063-015-0008-6, 2015.

755

Lucchi, R. G., Camerlenghi, A., Rebesco, M., Colmenero-Hidalgo, E., Sierro, F. J., Sagnotti, L., Urgeles, R., Melis, R., Morigi, C., Bárcena, M. A., Giorgetti, G., Villa, G., Persico, D., Flores, J. A., Rigual-Hernández, A. S., Pedrosa, M. T., Macri, P., and Caburlotto, A.: Postglacial sedimentary processes on the Storfjorden and Kveithola trough mouth fans: Significance of extreme glacimarine sedimentation, Global and Planetary Change, 111, 309-326, 10.1016/j.gloplacha.2013.10.008, 2013.

760

Mackensen, A., Schmiedl, G., Harloff, J., and Giese, M.: Deep-sea foraminifera in the South Atlantic Ocean: ecology and assemblage generation, Micropaleontology, 342-358, 1995.

Mangerud, J. and Gulliksen, S.: Apparent radiocarbon ages of recent marine shells from Norway, Spitsbergen, and Arctic Canada, Quaternary Research, 5, 263-273, 1975.

765

Melis, R., Carbonara, K., Villa, G., Morigi, C., Bárcena, M. A., Giorgetti, G., Caburlotto, A., Rebesco, M., and Lucchi, R. G.: A new multi-proxy investigation of Late Quaternary palaeoenvironments along the north-western Barents Sea (Storfjorden Trough Mouth Fan), Journal of Quaternary Science, 33, 662-676, 10.1002/jqs.3043, 2018.

Müller, J., Wagner, A., Fahl, K., Stein, R., Prange, M., and Lohmann, G.: Towards quantitative sea ice reconstructions in the northern North Atlantic: A combined biomarker and numerical modelling approach, Earth and Planetary Science Letters, 306, 137-148, 10.1016/j.epsl.2011.04.011, 2011.

770

Müller, J., Werner, K., Stein, R., Fahl, K., Moros, M., and Jansen, E.: Holocene cooling culminates in sea ice oscillations in Fram Strait, Quaternary Science Reviews, 47, 1-14, 10.1016/j.quascirev.2012.04.024, 2012.

Müller, P. J., Kirst, G., Ruhland, G., Von Storch, I., and Rosell-Melé, A.: Calibration of the alkenone paleotemperature index U37K′ based on core-tops from the eastern South Atlantic and the global ocean (60 N-60 S), Geochimica et cosmochimica Acta, 62, 1757-1772, 1998.

775

Nesje, A., Dahl, S. O., and Bakke, J.: Were abrupt Lateglacial and early-Holocene climatic changes in northwest Europe linked to freshwater outbursts to the North Atlantic and Arctic Oceans?, The Holocene, 14, 299-310, 10.1191/0959683604hl708fa, 2004.

780

Nobre, P., Veiga, S. F., Giarolla, E., Marquez, A. L., da Silva Jr, M. B., Capistrano, V. B., Malagutti, M., Fernandez, J. P., Soares, H. C., and Bottino, M. J.: AMOC decline and recovery in a warmer climate, Scientific Reports, 13, 15928, 2023.

Paus, A., Haflidason, H., Routh, J., Naafs, B. D. A., and Thoen, M. W.: Environmental responses to the 9.7 and 8.2 cold events at two ecotonal sites in the Dovre mountains, mid-Norway, Quaternary Science Reviews, 205, 45-61, 10.1016/j.quascirev.2018.12.009, 2019.

785

Pawłowska, J., Łącka, M., Kucharska, M., Pawlowski, J., and Zajączkowski, M.: Multiproxy evidence of the Neoglacial expansion of Atlantic Water to eastern Svalbard, Climate of the Past, 16, 487-501, 10.5194/cp-16-487-2020, 2020.

Rasmussen, T. L. and Thomsen, E.: The role of the North Atlantic Drift in the millennial timescale glacial climate
790   fluctuations, Palaeogeography, Palaeoclimatology, Palaeoecology, 210, 101-116,
        10.1016/j.palaeo.2004.04.005, 2004.

Rasmussen, T. L. and Thomsen, E.: Palaeoceanographic development in Storfjorden, Svalbard, during the
        deglaciation and Holocene: evidence from benthic foraminiferal records, Boreas, 44, 24-44,
        10.1111/bor.12098, 2015.

795   Rasmussen, T. L., Forwick, M., and Mackensen, A.: Reconstruction of inflow of Atlantic Water to Isfjorden,
        Svalbard during the Holocene: Correlation to climate and seasonality, Marine Micropaleontology, 94-95, 80-
        90, 10.1016/j.marmicro.2012.06.008, 2012.

Rasmussen, T. L., Thomsen, E., Ślubowska, M. A., Jessen, S., Solheim, A., and Koç, N.: Paleoceanographic
        evolution of the SW Svalbard margin (76°N) since 20,000 14C yr BP, Quaternary Research, 67, 100-114,
800   10.1016/j.yqres.2006.07.002, 2007.

Rebesco, M., Özmaral, A., Urgeles, R., Accettella, D., Lucchi, R. G., Rüther, D., Winsborrow, M., Llopart, J.,
        Caburlotto, A., Lantzsch, H., and Hanebuth, T. J. J.: Evolution of a high-latitude sediment drift inside a
        glacially-carved trough based on high-resolution seismic stratigraphy (Kveithola, NW Barents Sea),
        Quaternary Science Reviews, 147, 178-193, 10.1016/j.quascirev.2016.02.007, 2016.

805   Risebrobakken, B. and Berben, S. M. P.: Early Holocene Establishment of the Barents Sea Arctic Front, Frontiers
        in Earth Science, 6, 10.3389/feart.2018.00166, 2018.

Risebrobakken, B., Moros, M., Ivanova, E. V., Chistyakova, N., and Rosenberg, R.: Climate and oceanographic
        variability in the SW Barents Sea during the Holocene, The Holocene, 20, 609-621,
        10.1177/0959683609356586, 2010.

810   Risebrobakken, B., Dokken, T., Smedsrud, L. H., Andersson, C., Jansen, E., Moros, M., and Ivanova, E. V.: Early
        Holocene temperature variability in the Nordic Seas: The role of oceanic heat advection versus changes in
        orbital forcing, Paleoceanography, 26, PA4206, 10.1029/2011pa002117, 2011.

Rumohr, J., Blaume, F., Erlenkeuser, H., Fohrmann, H., Hollender, F.-J., Mienert, J., and Schäfer-Neth, C.:
        Records and processes of near-bottom sediment transport along the Norwegian-Greenland Sea margins during
815   Holocene and Late Weichselian (Termination I) times, The Northern North Atlantic: A Changing Environment,
        155-178, 2001.

Rüther, D. C., Bjarnadóttir, L. R., Junttila, J., Husum, K., Rasmussen, T. L., Lucchi, R. G., and Andreassen, K.:
        Pattern and timing of the northwestern Barents Sea Ice Sheet deglaciation and indications of episodic Holocene
        deposition, Boreas, 41, 494-512, 10.1111/j.1502-3885.2011.00244.x, 2012.

820   Sarnthein, M., Van Kreveld, S., Erlenkeuser, H., Grootes, P. M., Kucera, M., Pflaumann, U., and Schulz, M.:
        Centennial-to-millennial-scale periodicities of Holocene climate and sediment injections off the western
        Barents shelf, 75°N, Boreas, 32, 447-461, 10.1111/j.1502-3885.2003.tb01227.x, 2003.

Ślubowska-Woldengen, M., Koç, N., Rasmussen, T. L., Klitgaard-Kristensen, D., Hald, M., and Jennings, A. E.:
        Time-slice reconstructions of ocean circulation changes on the continental shelf in the Nordic and Barents Seas
825   during the last 16,000 cal yr B.P, Quaternary Science Reviews, 27, 1476-1492,
        10.1016/j.quascirev.2008.04.015, 2008.

Ślubowska, M. A., Koç, N., Rasmussen, T. L., and Klitgaard-Kristensen, D.: Changes in the flow of Atlantic water into the Arctic Ocean since the last deglaciation: Evidence from the northern Svalbard continental margin, 80°N, Paleoceanography, 20, PA4014, 10.1029/2005pa001141, 2005.

830 Smedsrud, L. H., Muilwijk, M., Brakstad, A., Madonna, E., Lauvset, S. K., Spensberger, C., Born, A., Eldevik, T., Drange, H., Jeansson, E., Li, C., Olsen, A., Skagseth, Ø., Slater, D. A., Straneo, F., Våge, K., and Årthun, M.: Nordic Seas Heat Loss, Atlantic Inflow, and Arctic Sea Ice Cover Over the Last Century, Reviews of Geophysics, 60, e2020RG000725, 10.1029/2020rg000725, 2021.

Stuiver, M., Reimer, P. J., and Reimer, R. W.: CALIB 8.2 [WWW program] at http://calib.org, accessed 2022-2-
835 25, 2022.

Svendsen, J. I., Elverhoi, A., and Mangerud, J.: The retreat of the Barents Sea Ice Sheet on the western Svalbard margin, Boreas, 25, 244-256, DOI 10.1111/j.1502-3885.1996.tb00640.x, 1996.

Szymczak-Żyła, M. and Lubecki, L.: Biogenic and anthropogenic sources of sedimentary organic matter in marine coastal areas: A multi-proxy approach based on bulk and molecular markers, Marine Chemistry, 239, 104069,
840 10.1016/j.marchem.2021.104069, 2022.

Telesiński, M. M., Przytarska, J. E., Sternal, B., Forwick, M., Szczuciński, W., Łącka, M., and Zajączkowski, M.: Palaeoceanographic evolution of the SW Svalbard shelf over the last 14 000 years, Boreas, 47, 410-422, 10.1111/bor.12282, 2018.

Tuckett, P. A., Ely, J. C., Sole, A. J., Lea, J. M., Livingstone, S. J., Jones, J. M., and van Wessem, J. M.: Automated
845 mapping of the seasonal evolution of surface meltwater and its links to climate on the Amery Ice Shelf, Antarctica, The Cryosphere Discussions, 2021, 1-35, 2021.

Von Grafenstein, U., Erlenkeuser, H., Müller, J., Jouzel, J., and Johnsen, S.: The cold event 8200 years ago documented in oxygen isotope records of precipitation in Europe and Greenland, Climate dynamics, 14, 73-81, 1998.

850 Vorren, T. O., Hald, M., and Thomsen, E.: Quaternary Sediments and Environments on the Continental-Shelf Off Northern Norway, Marine Geology, 57, 229-257, Doi 10.1016/0025-3227(84)90201-9, 1984.

Werner, K., Spielhagen, R. F., Bauch, D., Hass, H. C., and Kandiano, E.: Atlantic Water advection versus sea-ice advances in the eastern Fram Strait during the last 9 ka: Multiproxy evidence for a two-phase Holocene, Paleoceanography, 28, 283-295, 10.1002/palo.20028, 2013.

855 Werner, K., Müller, J., Husum, K., Spielhagen, R. F., Kandiano, E. S., and Polyak, L.: Holocene sea subsurface and surface water masses in the Fram Strait – Comparisons of temperature and sea-ice reconstructions, Quaternary Science Reviews, 147, 194-209, 10.1016/j.quascirev.2015.09.007, 2016.

Wollenburg, J. E. and Mackensen, A.: Living benthic foraminifers from the central Arctic Ocean: faunal composition, standing stock and diversity, Marine Micropaleontology, 34, 153-185, Doi 10.1016/S0377-
860 8398(98)00007-3, 1998.

You, D., Stein, R., Fahl, K., Williams, M. C., Schmidt, D. N., McCave, I. N., Barker, S., Schefuß, E., Niu, L., Kuhn, G., and Niessen, F.: Last deglacial abrupt climate changes caused by meltwater pulses in the Labrador Sea, Communications Earth & Environment, 4, 10.1038/s43247-023-00743-3, 2023.

865